



Cite as
Nano-Micro Lett.
(2023) 15:220

Received: 1 July 2023
Accepted: 28 August 2023
© The Author(s) 2023

Initiating Binary Metal Oxides Microcubes Electromagnetic Wave Absorber Toward Ultrabroad Absorption Bandwidth Through Interfacial and Defects Modulation

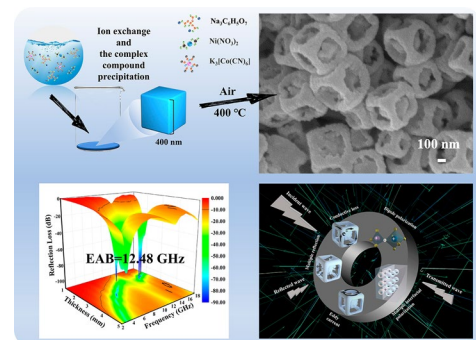
Fushan Li¹, Nannan Wu², Hideo Kimura¹, Yuan Wang³, Ben Bin Xu³ ✉, Ding Wang³, Yifan Li³, Hassan Algadi^{4,5}, Zhanhu Guo³ ✉, Wei Du¹ ✉, Chuanxin Hou¹ ✉

HIGHLIGHTS

- 3D cubic hollow core–shell NiCo₂O₄@C composites were synthesized.
- Oxygen vacancies were introduced into the prepared composites.
- Ultrabroad effective absorption bandwidth of 12.48 GHz was obtained.
- The absorption performance mechanism of NiCo₂O₄/C composites was investigated.

ABSTRACT Cobalt nickel bimetallic oxides (NiCo₂O₄) have received numerous attentions in terms of their controllable morphology, high temperature, corrosion resistance and strong electromagnetic wave (EMW) absorption capability. However, broadening the absorption bandwidth is still a huge challenge for NiCo₂O₄-based absorbers. Herein, the unique NiCo₂O₄@C core–shell microcubes with hollow structures were fabricated via a facile sacrificial template strategy. The concentration of oxygen vacancies and morphologies of the three-dimensional (3D) cubic hollow core–shell NiCo₂O₄@C framework were effectively optimized by adjusting the calcination temperature. The specially designed 3D framework structure facilitated the multiple reflections of incident electromagnetic waves and provided rich interfaces between multiple components, generating significant interfacial polarization losses. Dipole polarizations induced by oxygen vacancies could further enhance the attenuation ability for the incident EM waves. The optimized NiCo₂O₄@C hollow microcubes exhibit superior EMW absorption capability with minimum RL (RL_{\min}) of -84.45 dB at 8.4 GHz for the thickness of 3.0 mm. Moreover, ultrabroad effective absorption bandwidth (EAB) as large as 12.48 GHz (5.52–18 GHz) is obtained. This work is believed to illuminate the path to synthesis of high-performance cobalt nickel bimetallic oxides for EMW absorbers with excellent EMW absorption capability, especially in broadening effective absorption bandwidth.

KEYWORDS Electromagnetic wave absorber ; NiCo₂O₄@C Microcubes; Oxygen vacancy; Effective absorption bandwidth



✉ Ben Bin Xu, ben.xu@northumbria.ac.uk; Zhanhu Guo, zhanhu.guo@northumbria.ac.uk; Wei Du, duwei@ytu.edu.cn; Chuanxin Hou, chuanxin210@ytu.edu.cn

¹ School of Environmental and Material Engineering, Yantai University, No. 30 Qingquan Road, Yantai, Shandong 264005, People's Republic of China

² School of Material Science and Engineering, Shandong University of Science and Technology, Qingdao 266590, People's Republic of China

³ Mechanical and Construction Engineering, Faculty of Engineering and Environment, Northumbria University, Newcastle Upon Tyne NE1 8ST, UK

⁴ College of Materials Science and Engineering, Taiyuan University of Science and Technology, Taiyuan 030024, People's Republic of China

⁵ Department of Electrical Engineering, Faculty of Engineering, Najran University, 11001 Najran, Saudi Arabia



1 Introduction

The emergence of various wireless electronic devices was promoted by the rapid development of science and technology, provides people with convenience. However, the adverse effects of the operation and maintenance of sophisticated instruments, human organ damage, and even the survival of certain organisms were also produced by the electromagnetic radiation, which was called electromagnetic pollution [1–3]. For the sake of dealing with electromagnetic pollution, EMW absorbers have received numerous attentions due to their ability to weaken or/and dissipate EMW by converting them into other forms of energy [4–6]. The perfect electromagnetic wave absorber should satisfy the characteristics of strong absorption intensity, broad absorption bandwidth, thin matching thickness, and light weight. In the past decades, various materials have been carried out in EM absorption field [7–11], such as magnetic loss materials (*e.g.*, ferrite, metal alloys) and dielectric loss materials (*e.g.*, carbon-based materials, conductive polymers, and ceramics).

Among the plentiful EMW absorber materials, bimetallic cobalt–nickel oxide materials are receiving immense attentions due to their low synthesis cost, controlled morphology, and environmental friendliness. However, pure nickel cobaltate nanoparticles and nanosheets suffered from relatively poor EMW absorption ability with an RL_{\min} value of only -11 dB. The EMW absorption performance of pure nickel cobaltate nanoparticles is restricted due to impedance mismatch, which was caused by the poor magnetic loss capability [12].

To optimize the impedance matching to acquire satisfactory cobalt nickel bimetallic oxides absorber, two conventional strategies has been proposed. Designing and preparation of unique structure, including hollow porous structures, core–shell structures, etc., is considered as one effective route [13]. For example, the NiCo_2O_4 with porous hollow spherical structure and additional flower-like and flower-sphere structures were obtained by changing the type of surfactant, which exhibited an RL_{\min} value of -31.1 dB and an EAB value of 5.44 GHz at the thickness of 1.8 mm [14]. The uniquely designed structure with abundant microporous channels was proved to facilitate the multiple reflections and scatterings of incident EMW. Fabricating composites with multiple interfaces is believed to be another strategy to

promote the EMW absorption capacity by improving impedance matching and interface polarization ability simultaneously. Recently, defects-induced polarizations have been proved to improve the dielectric loss capacity effectively [15]. For example, $\text{Co}_3\text{O}_4@/\text{NiCo}_2\text{O}_4$ composites were synthesized and exhibited an EAB value of 4.88 GHz at 2.6 mm [14]. Hierarchical $\text{C}/\text{NiCo}_2\text{O}_4/\text{ZnO}$ composites were fabricated by hydrothermal, and sol–gel method, which delivered an EAB value of 4.32 GHz at a thickness of 2.4 mm [13, 16]. The existence of multi-component is conducive to inducing interface polarization, enhancing the dielectric loss ability [17].

Besides the two conventional strategies, defect engineering is also an effective tactic to improve the EMW absorption performance. Defect locations such as vacancies could trap carriers and disrupt the balance of charge distribution, resulting in defect polarization and loss of electromagnetic energy. NiCo_2O_4 absorbers with rich oxygen vacancies and functional groups were fabricated, and their EAB could cover the entire Ku-band [18]. Although extensive research have been carried out on NiCo_2O_4 absorber and achieved exceptional absorption performance [19], the demands for NiCo_2O_4 -based EMW absorbers with broadened absorption bandwidth are still a huge challenge.

Herein, the three-dimensional $\text{NiCo}_2\text{O}_4@/\text{C}$ hollow core–shell microcubes with rich oxygen vacancy defects were synthesized via facile chemical precipitation and following the calcination process. This special structure is forecast to provide multi-advantages to boost the EMW absorption performance. First, the special cubic hollow core–shell framework facilitates the entry of EMW and multiple reflections. Second, the introducing of carbon during the synthesis process facilitates the induction of interfacial polarization and reduces the density of the material to achieve a light-weight effect. Besides, the oxygen vacancy defects act as a dipole to induce dipole polarization and effectively enhance the dielectric loss capacity of the absorber. In terms of the synergistic effect of hollow microstructure, multi-component, and defect engineering, the optimized $\text{NiCo}_2\text{O}_4@/\text{C}$ absorber showed an RL_{\min} value of -84.45 dB and ultra-broad EAB value as large as 12.48 GHz (5.52–18 GHz), which is the largest among the current reports. This work tremendously broadens the effective absorption bandwidth of NiCo_2O_4 -based absorbers, which will accelerate its practical application in EM absorption fields.

2 Experimental Section

2.1 Materials

Sodium citrate ($C_6H_5O_7Na_3$, $\geq 98.0\%$), Nickel nitrate ($Ni(NO_3)_2 \cdot 6H_2O$, $\geq 99.0\%$), and Potassium hexacyanocobaltate (III) ($C_6CoK_3N_6$, $\geq 99.9\%$) were provided by Rgent, Dingshengxin and Macklin, respectively. All analytical reagents were used directly without further purification.

2.2 Synthesis of $NiCo_2O_4@C$ Composites

The Ni–Co–PBA nanocubes were obtained by a typical precipitation method. 2.4 mmol $C_6H_5O_7Na_3$ and 1.6 mmol $Ni(NO_3)_2 \cdot 6H_2O$ were dissolved into 60 mL of deionized (DI) water, stirring for 10 min to form uniform solution I. Meanwhile, 1.0 mmol $C_6CoK_3N_6$ was dissolved into 40 mL of DI water to form uniform solution II. Then, the solution I and II were mixed under stirring for 10 min. The acquired mixed solution was kept for 12 h at room temperature. The precipitation products were collected by centrifugation and washing with water and ethanol several times and dried at 60 °C for 12 h. The final products were obtained after heat treatment of Ni–Co–PBA nanocubes precursor at 360, 380, 400 and 420 °C in air for 2 h with a heating rate of 2 °C min^{-1} , which marked as NCO-1, NCO-2, NCO-3 and NCO-4, respectively.

2.3 Characterization

The phase structure was characterized by X-ray diffraction (XRD) using a Rigaku D/max-3C. The morphologies and microstructures were analyzed by a scanning electron microscope (SEM, JSM-7610F, Japan) and a transmission electron microscope (TEM, TF20), respectively. The composition and valence of elements of the prepared $NiCo_2O_4$ nanomaterials were determined by X-ray photoelectron spectrometer (XPS, Thermo Scientific K-Alpha), Raman spectrometer (Horiba LabRAM HR Evolution), and TGA/DSC system (Netzsch STA 449 F3). The magnetic characters of the as-prepared samples were observed via a vibrating sample magnetometer (VSM, LakeShore7404, USA) at room temperature. The specific surface and pore size distribution were analyzed by nitrogen adsorption–desorption isotherms (ASAP 2460). To demonstrate the presence of oxygen vacancies, the samples

were tested using electron paramagnetic resonance spectroscopy (EPR, Bruker EMXplus-6/1, Germany).

2.4 Electromagnetic Measurements

To evaluate the electromagnetic parameters, a vector network analyzer (3656D) was utilized between 2 and 18 GHz. An appropriate amount of the prepared sample and paraffin was mixed by heating and stirring, and transferred into in the mold to form a test ring ($\Phi_{outer} = 7.00$ mm, $\Phi_{inter} = 3.04$ mm, thickness = 2.0 mm) with a filling ratio of 20, 30, and 40%.

3 Results and Discussion

The synthesis route of the 3D cubic hollow core–shell $NiCo_2O_4@C$ framework composites with oxygen vacancy defects is schematically described in Fig. 1a. The dissociated Ni^{2+} coordinated with $[Co(CN)_6]^{3-}$ to produce large number of Ni–Co–PBA nanoclusters, which aggregated into primary nanoparticles at supersaturations by van der Waals forces in an oriented manner. During this process, citrate will adsorb on the surface of the nanoparticles to control the binding rate. The morphology of the prepared composites was controlled by changing the amount of citrate and precipitation time. The morphologies of NiCo–PBA precursor and the 3D cubic hollow core–shell $NiCo_2O_4@C$ composites are investigated by SEM and TEM measurements, which are shown in Figs. 1 and S1–S5. The NiCo–PBA precursor in Fig. 1b shows a uniform cube structure with an average size of approximately 400 nm. During the following heat treatment process, with the increasing temperature, the decomposition of –CN– is occurred, and the precursor cube undergoes a series of changes, the individual faces gradually depressed (Fig. 1c, d), forming a 3D $NiCo_2O_4@C$ hollow core–shell microcubes framework (Fig. 1e, f), and eventually, the structure collapses (Fig. 1g). The $NiCo_2O_4@C$ composites exhibit uniformly hollow core–shell microcubes structure, which inherited the size of NiCo–PBA precursor. The TEM is carried out to observe the microstructure of $NiCo_2O_4@C$ composites. Figure 1h, i further identifies the hollow core–shell framework of the prepared composites. The lattice fringe spacings of 0.47, 0.24, and 0.25 nm in Fig. 1j are labeled as (111), (222), and (311) crystal planes of $NiCo_2O_4$. Furthermore, the TEM-based (Fig. 1k)

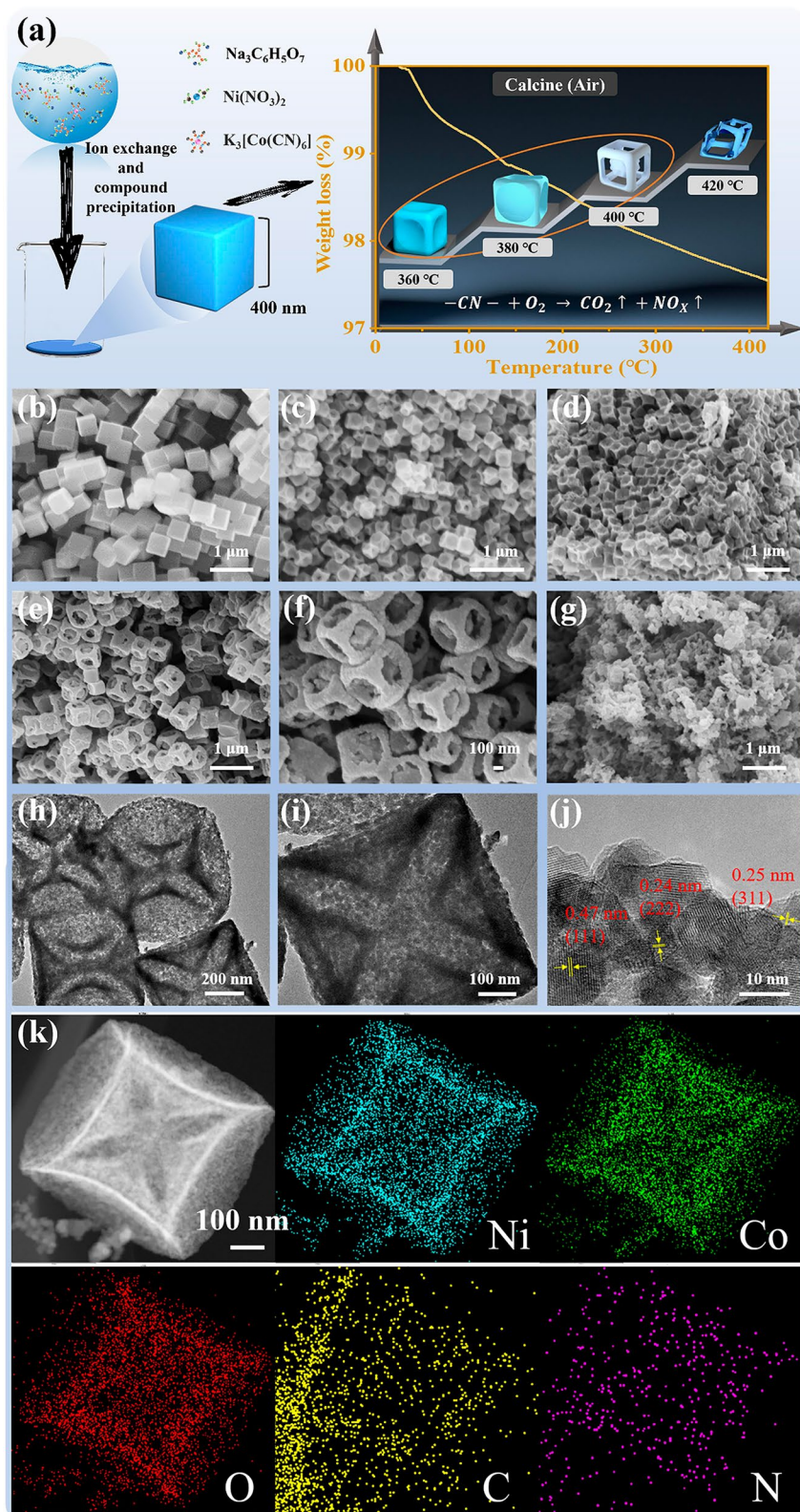


Fig. 1 a Schematic illustration of the preparation route of the 3D hollow NiCo_2O_4 microcubes. SEM images of b Ni-Co-PBA, c NCO-1, d NCO-2, e-f NCO-3 and g NCO-4; h-j TEM images and k TEM-based EDS mapping of NCO-3

and SEM-based EDS mapping result (Fig. S6) shows the uniform dispersion of Ni, Co, C, O, and N element in the NCO-3 composites. The results illustrate the transition of the NiCo-PBA precursor to NiCo_2O_4 .

The phase structure and crystallinity of precursors and NCO is characterized by XRD (Figs. 2a and S7). The Ni-Co PBA precursors in Fig. S1 is detected as $\text{Ni}_3[\text{Co}(\text{CN})_6]_2 \cdot 12\text{H}_2\text{O}$ (JCPDS NO. 89–3738). Then the Ni-Co PBA precursors transform into $\text{NiCo}_2\text{O}_4/\text{C}$ hybrids, where the obvious diffraction peaks located at the 2θ of 18.91° , 31.15° , 36.70° , 44.62° , 59.10° and 64.98° in Fig. 2a are attributed to the (111), (220), (311), (400), (511), and (440) planes of NiCo_2O_4 (PDF #NO.20–0781) [20]. These results further prove the successful preparation of $\text{NiCo}_2\text{O}_4/\text{C}$ microcubes.

Figure 2b shows the Raman spectra of the prepared composite, where the four distinct stretching vibration peaks at 184 , 463 , 510 , and 651 cm^{-1} are detected as F_{2g} , E_g , F_{2g} , and A_{1g} signals of NiCo_2O_4 orderly [21, 22], which further prove the formation of NiCo_2O_4 . The peaks at ~ 510 and $\sim 651\text{ cm}^{-1}$ are in connection with the vibration of oxygen ions (tetrahedral) and Co–O (octahedral), separately. The differences in F_{2g} and A_{1g} peak positions for the four samples, where 517 and 660 cm^{-1} for NCO-1, 509 and 656 cm^{-1} for NCO-2 and 509 and 651 cm^{-1} for NCO-4, is attribute to the disruption of lattice symmetry by defects caused during the calcination process. The peaks move towards lower frequencies with the increase of heat treatment temperature that are inferred to promote the generation of more oxygen vacancy defects, which induces defect polarization to enhance the electromagnetic absorption property [23]. To explore the detailed microstructure characteristics of the prepared composites, the N_2 adsorption/desorption isotherms and pore size distribution curve of NCO-3 are displayed in Fig. 2c. The typical type IV isotherms can be observed directly, indicating the presence of mesoporous structure [24–26]. The specific surface area of NCO-3 is calculated to be *ca.* $11.2\text{ m}^2\text{ g}^{-1}$, and the pore size mainly distributes between 1 and 150 nm .

The valence state and chemical composition of the prepared $\text{NiCo}_2\text{O}_4/\text{C}$ hybrids is explored by the XPS test (Fig. 2d–k). The XPS spectra of NCO-3 illustrate the existing elements of C 1s, Co 2p, Ni 2p, and O 1s, which further confirm the successful synthesis of $\text{NiCo}_2\text{O}_4/\text{C}$ composites. The three split peaks in the spectra of C 1s in Fig. 2e are attributed to the C–C (284.6 eV), C–O (285.6 eV), and O–C=O (288.5 eV), respectively [27]. The Co 2p spectra (Fig. 2f) can be fitted to two spin-orbit doublets characteristics of Co^{2+} (780.98 and

796.5 eV) and Co^{3+} (788 and 805 eV), accompanying two satellite peaks (788 and 805 eV) [28, 29]. Meanwhile, the Ni 2p emission spectra (Fig. 2g) can be fitted to two spin-orbit doublets features of Ni^{2+} and Ni^{3+} , accompanying two shakeup satellites [18]. Similarly, the spectra of Ni 2p are composed of two satellite peaks (862 and 880 eV) and two spin-orbit doublets features of Ni^{2+} (854 and 872 eV) and Ni^{3+} (856 and 874 eV) [30]. The O 1s spectrum consists of four categories of oxygen species (Fig. 2h–k). The peaks at 529.5 and 531.2 eV accord to the Ni–O and Co–O bond, respectively [31]. Simultaneously, the peak at 530.7 eV is related to oxygen vacancy, illustrating the presence of oxygen vacancy defects, consistent with the electron paramagnetic resonance (EPR) test results (Fig. S8). In our previous study, it was been proved that the content of oxygen vacancy defects is positively correlated with the electromagnetic wave absorption performance [32]. Therefore, the relative oxygen vacancy content of the $\text{NiCo}_2\text{O}_4/\text{C}$ hybrids was calculated and compared based on the proportion of the integral area in Table S1. The NCO-3 presents the highest content of oxygen vacancies, which is favorable to generate dipole polarizations, illustrating the content of oxygen vacancy defects increases by the heat treatment temperature, and also influenced by structural integrity of the composites. Besides, the peak in 532.5 eV is indexed to the adsorbed water on the material surface [33].

To further detect the existence of carbon matrix in the prepared composites, the TGA measurement of NCO-3 is displayed in Fig. S9. In the process of heating, the mass of the sample gradually decreases; the weight change may be caused by the evaporation of water, the combustion of carbon, the decomposition and oxidation of the –CN– bond that generates carbon and nitrogen oxide gas and escapes into the air, and the conversion of NiCo_2O_4 into NiO and Co_3O_4 after heating up to 500°C . in which Co^{2+} is oxidized to Co^{3+} , and Ni^{3+} and O_2 molecules are reduced to Ni^{2+} and O^{2-} [34].

The static magnetic property of the NiCo_2O_4 is tested at room temperature and shown in Fig. 2l. The coercively values of the absorbers are all around 251 Oe , indicating the similar storage capacity of magnetic energy in this series of samples [35]. The saturation magnetization (M_s) value gradually decreases with increasing temperature, and the maximum M_s was only 3.45 emu g^{-1} for the NCO-1, which illustrate the hysteresis loss with low saturation magnetization contributes little to the magnetic loss of the absorbers. [36]

EPR results in Fig. S8 prove the existence of oxygen vacancy (O_v) [20], which depends on Eq. (1) [24]:

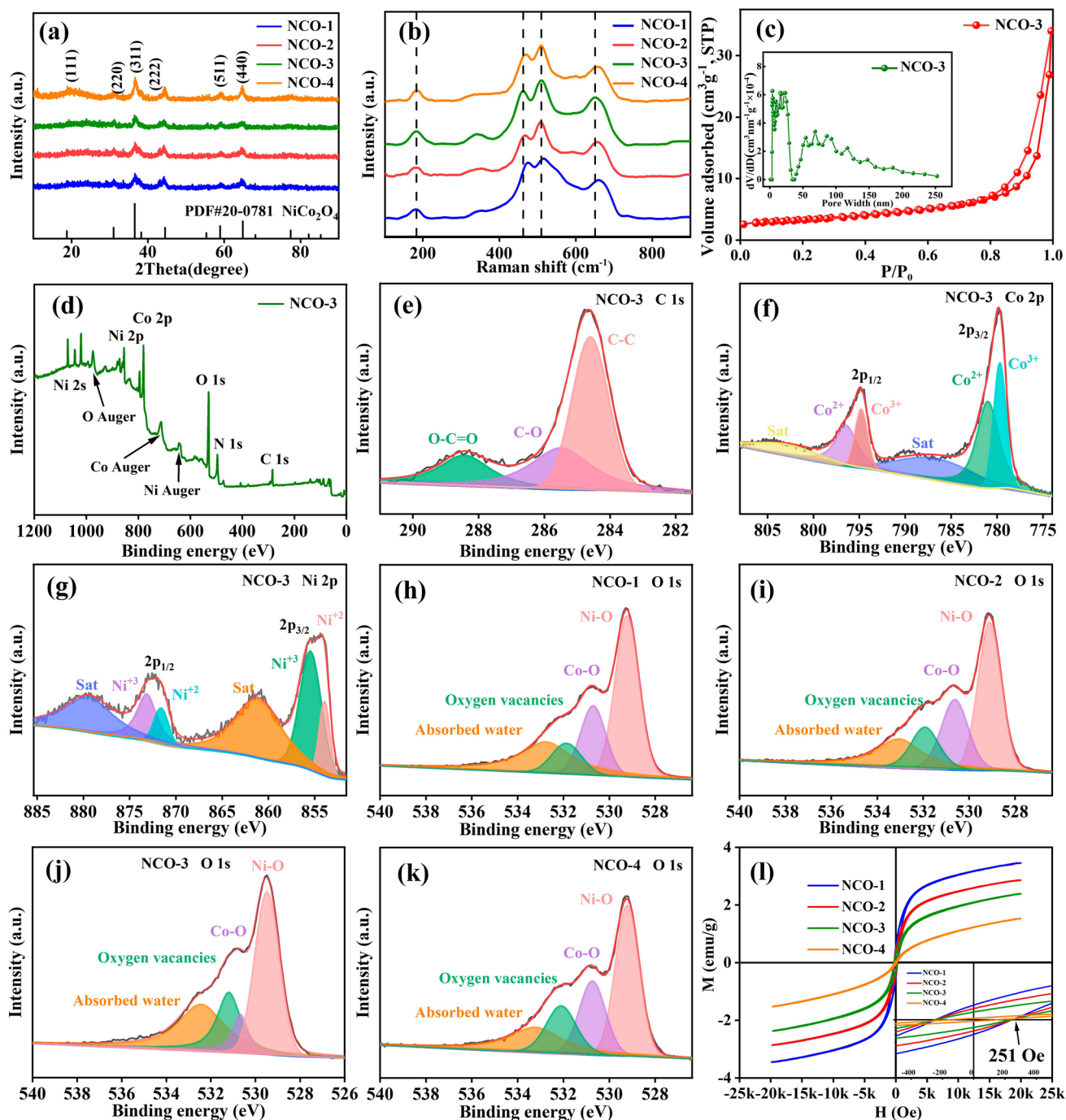


Fig. 2 **a** XRD patterns, **b** Raman test of the prepared NCO; **c** Nitrogen adsorption/desorption isotherms and the pore size distributions, **d** XPS spectra of NCO-3, high-resolution XPS spectra for **e** C 1s, **f** Co 2p and **g** Ni 2p of NCO-3; XPS spectra of O 1s of **h** NCO-1, **i** NCO-2, **j** NCO-3 and **k** NCO-4; **l** the magnetization curve of NCO

$$h\nu = g\beta B \quad (1)$$

where h represents Planck's constant, ν is frequency, g means constant, β means Bohr magneton, and B mean applied

magnetic field. The recognized g value of materials with O_V is ca. 2.00, which is associated with the nature of radical. The g value of the $NiCo_2O_4/C$ hybrids is calculated to be 2.00477, 2.00466, 2.00497, and 2.00494, respectively,

which further indicate the occurrence of oxygen vacancy. The oxygen vacancies act as point defects, which will trap electrons and disrupt the equilibrium distribution of charges, leading to polarization and loss of electromagnetic energy under the altering electric field.

The EMW absorbing properties of the synthesized NiCo₂O₄/C composites (with filling ratio of 40%) are dominated by the complex permittivity ($\epsilon_r = \epsilon' - j\epsilon''$) and

permeability ($\mu_r = \mu' - j\mu''$). The electromagnetic parameters of the absorbers are obtained from the vector network analyzer test that shown in Fig. 3. The real parts of permittivity (ϵ'), decreases accompanied by the increasing frequency, and some fluctuations are observed in the curve (Fig. 3a). The imaginary part (ϵ'') of the complex permittivity (Fig. 3b) and dielectric loss tangent (Fig. 3c) presents

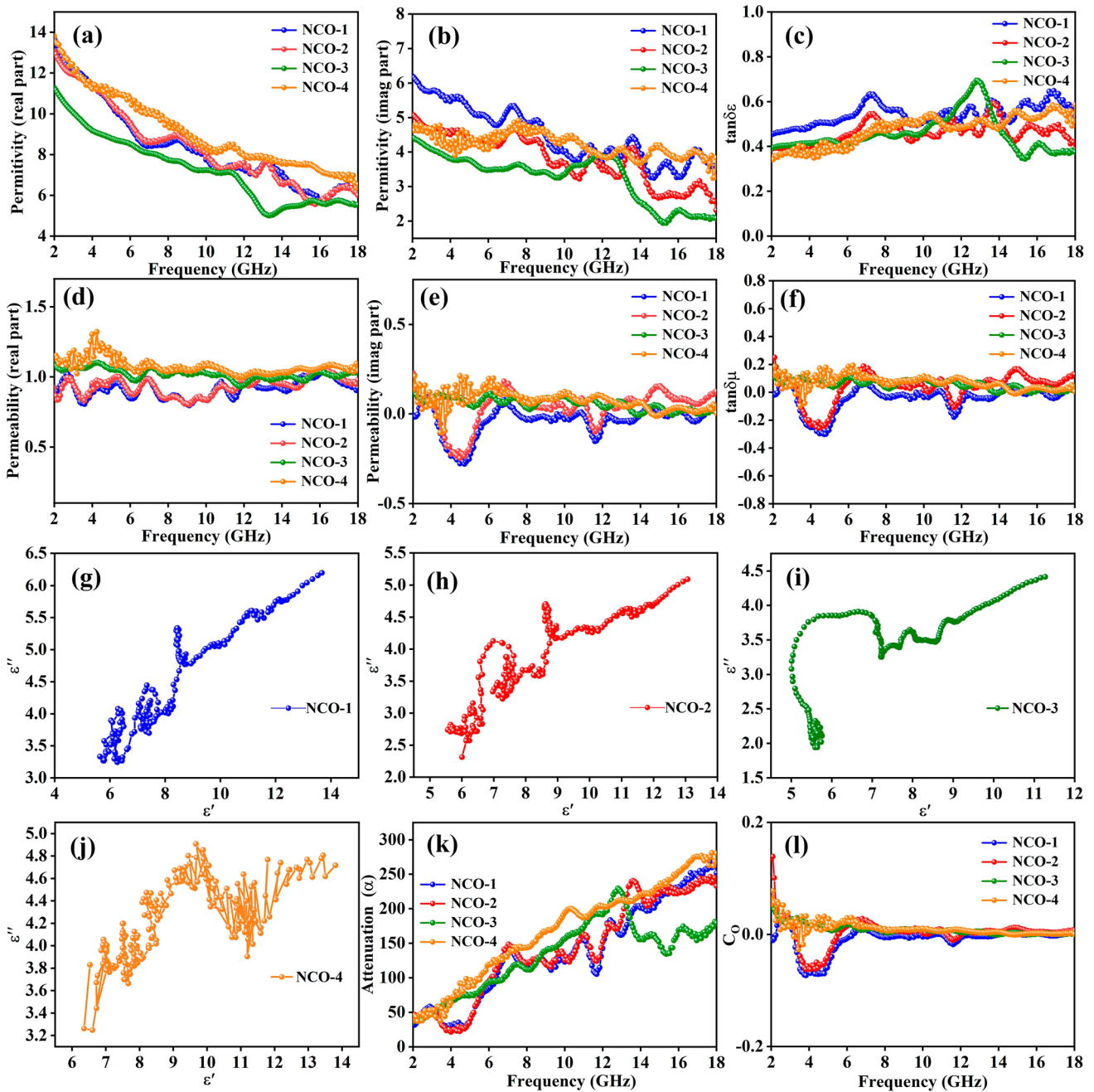


Fig. 3 Frequency dependence of **a** ϵ' and **b** ϵ'' ; **c** $\tan \delta\epsilon$ and **d** μ' ; **e** μ'' ; **f** $\tan \delta\mu$; **g–j** Cole–Cole semicircles; **k** Attenuation constant α , and **l** Q of prepared composites

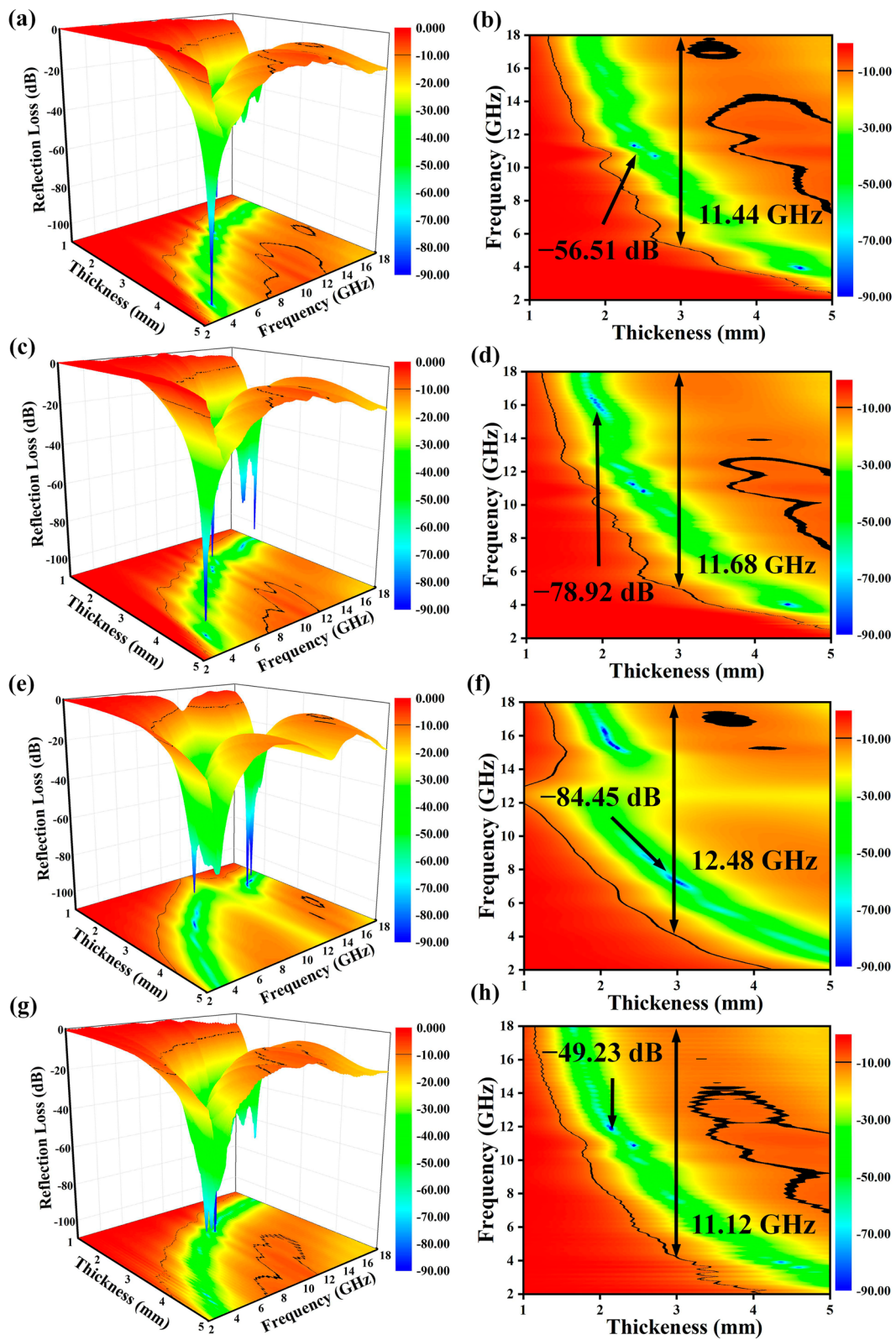


Fig. 4 3D, 2D color map at different matching thicknesses of **a, b** NCO-1, **c, d** NCO-2, **e, f** NCO-3 and **g, h** NCO-4

multiple vibrational peaks from 6.5 to 18 GHz, indicating the existence of Debye relaxation, which corresponds well with the results of Cole–Cole semicircles (Fig. 3g–j). The dipole polarization formed in the prepared absorbers due to the abundant oxygen vacancies. And interfacial polarization between heterogeneous interfaces (NiCo₂O₄, carbon, and air) is inferred to contribute to satisfactory properties.

The complex permeability of the absorbers fluctuates in a low-value range (0.79 to 1.32 and –0.28 to 0.21, respectively) for both μ' and μ'' (Fig. 3d, e), which indicates a relatively poor magnetic loss capability [6]. The multiple resonance peaks (Fig. 3f) mainly originate from exchange resonance and natural resonance. Besides, eddy current loss is also an essential magnetic loss mechanism, which is described by the eddy current coefficient ($C_0 = \mu''(\mu')^2 f^{-1}$) [37]. As shown in Fig. 3l, the C_0 of the NiCo₂O₄/C absorbers is almost a constant in the range of 6 to 18 GHz, suggesting a nonnegligible role of eddy current loss in the magnetic loss behavior.

The RL values are calculated according to transmission line theory, as shown in Eqs. 2 and 3 [38]:

$$Z_{in} = Z_0 \sqrt{\frac{\mu_r}{\epsilon_r} \tanh \left[j \left(\frac{2\pi f d}{c} \right) \sqrt{\mu_r \epsilon_r} \right]} \quad (2)$$

$$RL = 20 \lg \left| \frac{Z_0 - Z_{in}}{Z_0 + Z_{in}} \right| \quad (3)$$

where Z_{in} means the input impedance of the absorber, Z_0 means the impedance of free space, ϵ_r and μ_r represent the complex permittivity and complex permeability, respectively, f means the frequency of the incident electromagnetic wave, d is the thickness and c is the speed of the EMW. The RL value less than –10 dB illustrates more than ninety percent of the incident EMW could be absorbed and the corresponding frequency range with RL lower than –10 dB is considered as EAB [22].

The EMW absorption performance of the as-synthesized NiCo₂O₄@C microcubes is presented in Figs. 4 and 5. The results illustrate NiCo₂O₄@C microcubes present outstanding EMW absorption performance in terms of the calculated RL and EAB values. An EAB value of 11.44 GHz for NCO-1 is obtained at 3.0 mm and the RL_{min} value reaches –56.51 dB at the thickness of 2.5 mm (Figs. 4a, b and 5a). For NCO-2, the EAB value increases to 11.68 GHz at 3.0 mm, and the RL_{min} value of –78.92 dB is obtained at 2.0 mm (Figs. 4c, d and 5b). A satisfactory EAB value of 11.12 GHz obtained at 3.0 mm and RL_{min} value of –49.23 dB at 2.0 mm are

Table 1 Comparison of EMW absorbing properties of NiCo₂O₄-based absorbers

Absorbers	RL_{min} (dB)	EAB (GHz)	References
NiCo ₂ O ₄	–32.56	5.81	[1]
C/NiCo ₂ O ₄ /ZnO	–43.61	4.32	[13]
NiCo ₂ O ₄	–37.00	4.64	[14]
Co ₃ O ₄ @ NiCo ₂ O ₄	–34.42	4.88	[15]
NiCo ₂ O ₄	–42.80	6.08	[18]
NiCo ₂ O ₄	–38.9	6.26	[20]
NiO/ NiCo ₂ O ₄	–48.10	5.84	[23]
NiCo ₂ O ₄	–47.01	2.98	[24]
C@NiCo ₂ O ₄	–39	4.16	[30]
NiCo ₂ O ₄ /Co ₃ O ₄ /NiO	–28.63	4.72	[31]
NiCo ₂ O ₄ /HCNT	–55.9	4.8	[33]
NiO/ NiCo ₂ O ₄	–57.40	6.08	[36]
MWCNT@ NiCo ₂ O ₄	–41.5	5.0	[46]
NiCo ₂ O ₄	–49.78	7.10	[47]
NiCo ₂ O ₄ @C	–84.45	12.48	This work

obtained for NCO-4, respectively (Figs. 4g, h and 5d). Encouragingly, an ultra-large EAB value as broad as 12.48 GHz (5.52 to 18 GHz) and RL_{min} value of –84.45 dB at the thickness of 3.0 mm (Figs. 4e, f and 5c), which is the largest among the NiCo₂O₄-based absorbers (Table 1). It is worth noting that none RL value for EMW absorbers at multiple matched thicknesses beyond –10 dB at 18 GHz, indicating that the absorbers display potential absorption capability in the higher frequency range. The absorption performance of the four EMW absorbers is compared in more detail by reducing the matching thickness from 0.5 to 0.2 mm, as shown in Fig. 5e–l, where the EAB of all the four EMW absorbers exceed 10 GHz and RL_{min} values exceed –20 dB (losing 99% of the incident electromagnetic wave) at these matched thicknesses. Figure 5m, n shows the comparison of EMW Absorption performance for all absorbers at the thickness of 3 and 5 mm, respectively, which further prove the NCO-3 possessed the optimum EAB value. Meanwhile, the EAB value even reaches 14.96 GHz at the thickness of 5.0 mm.

In order to investigate the attenuation mechanism for the excellent EMW absorption, the attenuation constant (α) is evaluated using Eq. 4 [39]:

$$\alpha = \frac{\sqrt{2}\pi f}{c} \times \sqrt{\mu''\epsilon'' - \mu'\epsilon' + \sqrt{(\mu'\epsilon'' + \mu''\epsilon')^2 + (\mu''\epsilon'' - \mu'\epsilon')^2}} \quad (4)$$

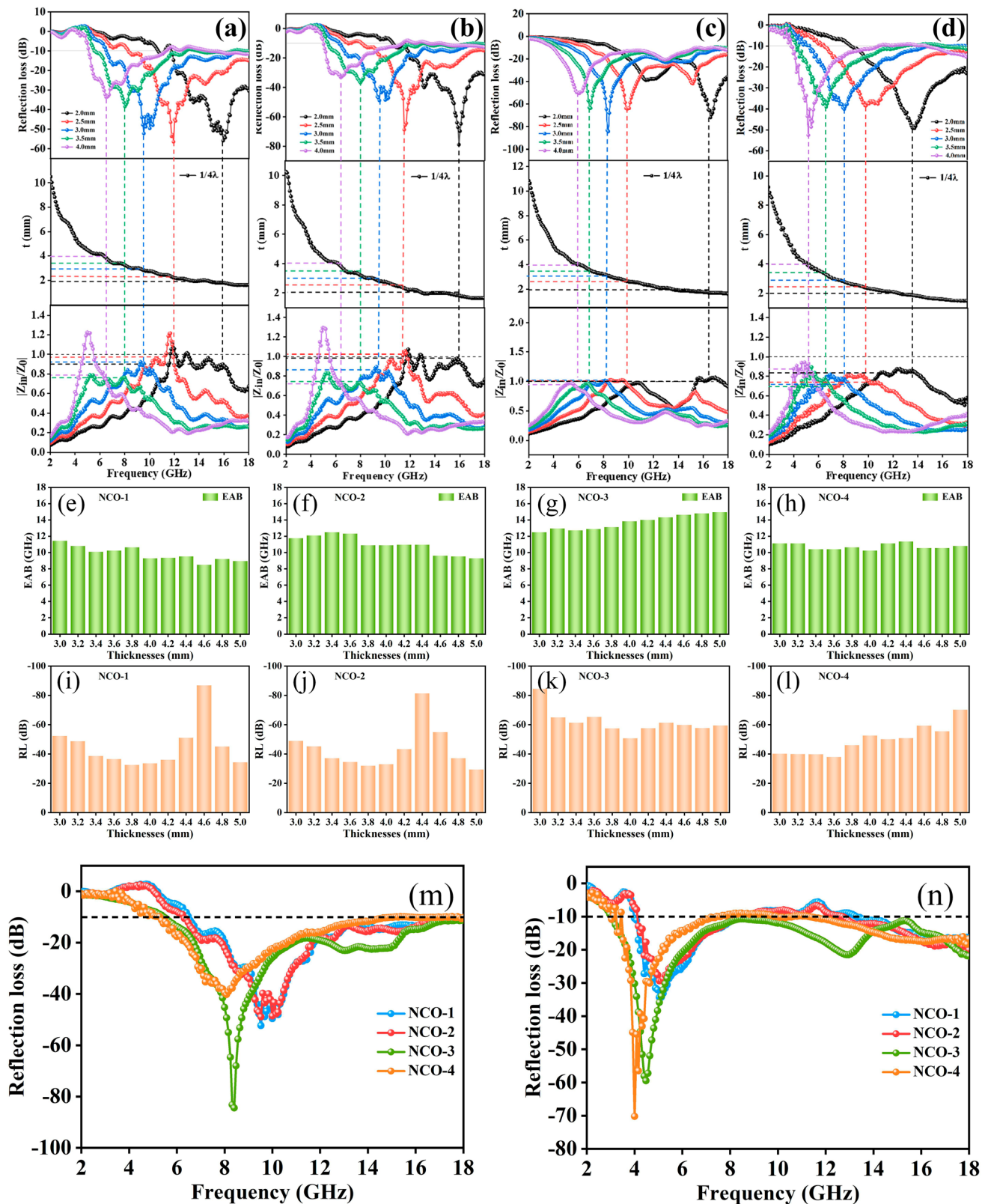


Fig. 5 RL values vs. frequency at different thicknesses, the simulations of the absorber thickness vs. peak frequency under $1/4$ conditions, and the impedance matching characteristic for **a** NCO-1, **b** NCO-2, **c** NCO-3, and **d** NCO-4. Comparison of **e-h** EAB values and **i-l** RL_{min} at a matched thickness of 3–5 mm. Comparison of EMW absorption performance at a thickness of **m** 3 mm and **n** 5 mm

Figure 3k displays the α -values of the four prepared absorbers, which shows the result of $\text{NCO-4} > \text{NCO-2} > \text{NCO-1} > \text{NCO-3}$. Theoretically, NCO-4 should present the optimum EMW absorption capacity, but the impedance matching factor should be considered.

For exploring deeper into the cause of the excellent EM wave dissipation behavior of the $\text{NiCo}_2\text{O}_4/\text{C}$ absorbers, the impedance matching characteristic ($Z = |Z_{in}/Z_0|$) is computed and exhibited in Figs. 4 and 5. Typically, the better the impedance matching for the absorber [40], the less reflection the incident EMW. The results show that the impedance matching of the prepared absorbers floats around 1.0 at a suitable matching thickness [41]. By further comparative analysis, NCO-3 displays the most outstanding impedance match. Based on the synergistic effect of impedance matching and attenuation constants, the NCO-3 presents a superior EMW absorption capability.

Furthermore, EMW absorption capability of NCO-3 with a filling ratio of 20% and 30% was tested, which are presented in Figs. S10–S12. The NCO-3 with filling ratio of 20% exhibits an EAB of 5.44 GHz at 3.0 mm and an RL_{\min} value of -20.44 dB at 3.5 mm and NCO-3 with filling ratio of 30% exhibits an EAB value of 4.96 GHz

at 2.5 mm and an RL_{\min} value of -46.02 dB at 5.0 mm, respectively, which demonstrates noteworthy impact of the filling ratio for EMW absorption capability.

For better understanding of the outstanding EMW absorption performance of the $\text{NiCo}_2\text{O}_4/\text{C}$ absorber, the quarter wavelength theory was applied by Eq. 5 [42]:

$$t_m = \frac{n\lambda}{4} = \frac{nc}{4f_m \sqrt{|\epsilon_r||\mu_r|}} \quad (n = 1, 3, 5, \dots) \tag{5}$$

where t_m and f_m mean the optimal thickness and frequency of the absorbers. The matching results of RL_{\min} , thickness, and frequency are shown in Fig. 5. The intersection of the dashed line and the t-curve indicate the matching thickness vs. the peak frequency collected in Fig. 5a–d. The positions of these data are around the $1/4 \lambda$, indicating these absorbers are in accordance with the quarter wavelength theory. Therefore, incident and reflected EMW would be canceled by each other in the interface of air-absorbers as the phase difference of 180° , maximizing the EMW attenuation ability.

The outstanding EMW dissipation of NCO-3 with an ultrabroad EAB value of 12.48 GHz is achieved, and the attenuation mechanisms are summarized in Fig. 6. The outstanding impedance matching characteristics allow

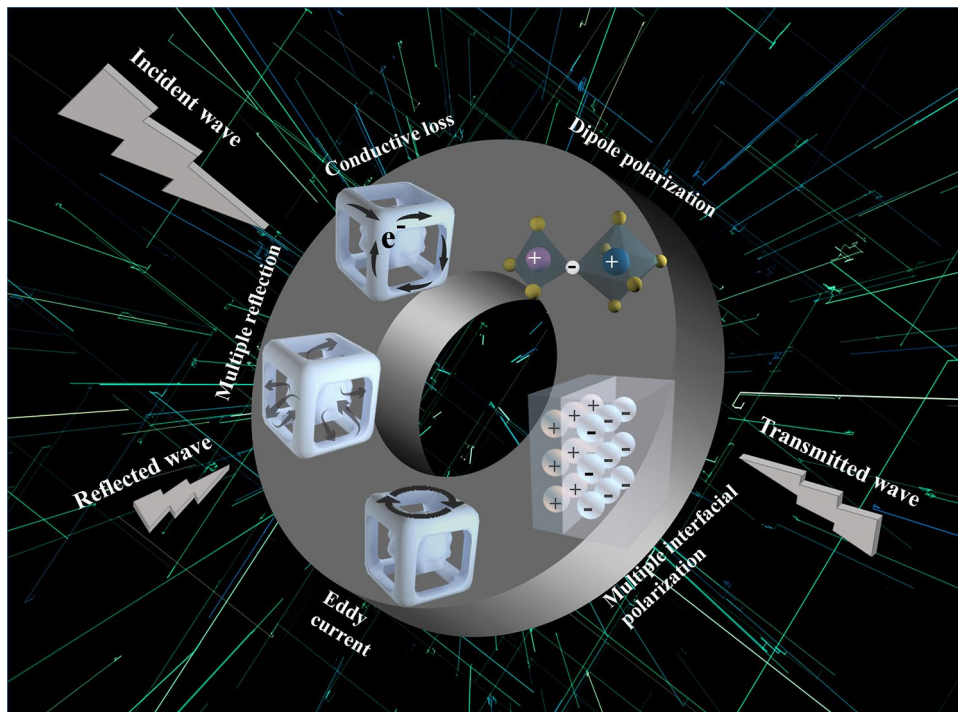


Fig. 6 Schematic illustration of EMW absorption mechanism

EMW to enter the absorbers to the greatest extent firstly. Secondly, these controllable oxygen vacancy defects act as dipoles and induce dipole polarization. The dipoles would change their arrangement from disorder to order when an electric field is applied, and the incident EMW will be effectively dissipated during this period [43]. Thirdly, the existence of eddy current loss and interface polarization induced by the accumulation of different charges at the heterogeneous interfaces, are beneficial to the loss effect of EMW. Fourthly, the different binding energy for electric charges on the sides of the interface leads to differences in the amount of charge migration in and out of electromagnetic fields, resulting in interface polarization. Finally, when the EMW enters the inside framework, multiple reflections between the gaps are happened to increase the propagation path and then dissipate the EM waves [44, 45]. Furthermore, macroscopic current would be generated in the absorber under an applied electromagnetic field, and the EMW would be converted into heat energy based on the Joule theory.

4 Conclusions

In summary, the 3D core-shell NiCo₂O₄@C hollow microcubes are synthesized by the environmentally-friendly sacrificial template method. The oxygen vacancy defects are introduced into the special framework due to the sensitive response of NiCo₂O₄ to temperature changes. The evolution of morphology with temperature affected the density, distribution of heterogeneous interfaces, and the content of oxygen vacancy defects of the prepared composites, thus affecting the impedance matching and attenuation capability of the absorber. Benefiting from the synergistic EMW absorption mechanisms, including multiple reflections and scattering induced by the abundant pores, interfacial polarization induced by multiple components, dipole polarization induced by the defects, conductive loss, and eddy current loss, the optimized NCO-3 presented ultra-broad EAB value of 12.48 GHz (5.52 to 18 GHz), and RL_{\min} value of -84.45 dB at 8.4 GHz, covering the entire X and Ku band and even extends to the K band, which is the broadest among the reported NiCo₂O₄-based absorbers. It is believed that this report could illuminate the route for applications of high-performance NiCo₂O₄-based and other transition metal oxides-based EMW absorbers.

Acknowledgements This work was supported by Natural Science Foundation of Shandong Province (ZR2022ME089), National Natural Science Foundation of China (52207249) and Yantai Basic Research Project (2022JCYJ04).

Funding Open access funding provided by Shanghai Jiao Tong University.

Declarations

Conflict of interest The authors declare that they have no known competing financial interests or personal relationships that could have appeared to influence the work reported in this paper.

Open Access This article is licensed under a Creative Commons Attribution 4.0 International License, which permits use, sharing, adaptation, distribution and reproduction in any medium or format, as long as you give appropriate credit to the original author(s) and the source, provide a link to the Creative Commons licence, and indicate if changes were made. The images or other third party material in this article are included in the article's Creative Commons licence, unless indicated otherwise in a credit line to the material. If material is not included in the article's Creative Commons licence and your intended use is not permitted by statutory regulation or exceeds the permitted use, you will need to obtain permission directly from the copyright holder. To view a copy of this licence, visit <http://creativecommons.org/licenses/by/4.0/>.

Supplementary Information The online version contains supplementary material available at <https://doi.org/10.1007/s40820-023-01197-0>.

References

1. Q. Chang, H.S. Liang, B. Shi, X.L. Li, Y.T. Zhang et al., Ethylenediamine-assisted hydrothermal synthesis of NiCo₂O₄ absorber with controlled morphology and excellent absorbing performance. *J. Colloid Interface Sci.* **588**, 336–345 (2021). <https://doi.org/10.1016/j.jcis.2020.12.099>
2. J. Guo, Z.R. Chen, X.J. Xu, X. Li, H. Liu et al., Enhanced electromagnetic wave absorption of engineered epoxy nanocomposites with the assistance of polyaniline fillers. *Adv. Compos. Hybrid Mater.* **5**(3), 1769–1777 (2022). <https://doi.org/10.1007/s42114-022-00417-2>
3. J.C. Ruan, Z.X. Chang, H.W. Rong, T.S. Alomar, D.P. Zhu et al., High-conductivity nickel shells encapsulated wood-derived porous carbon for improved electromagnetic interference shielding. *Carbon* **213**, 118208 (2023). <https://doi.org/10.1016/j.carbon.2023.118208>
4. N.N. Wu, B.B. Zhao, X.Y. Chen, C.X. Hou, M.N. Huang et al., Dielectric properties and electromagnetic simulation of molybdenum disulfide and ferric oxide-modified Ti₃C₂T_x MXene hetero-structure for potential microwave. *Adv. Compos. Hybrid Mater.* **5**(2), 1548–1556 (2022). <https://doi.org/10.1007/s42114-022-00490-7>

5. J. Guo, S.H. Xi, Y.X. Zhang, X. Li, Z.R. Chen et al., Biomass based carbon materials for electromagnetic wave absorption: a mini-review. *ES Food Agrofor.* **13**, 900 (2023)
6. N.N. Wu, B.B. Zhao, J.Y. Liu, Y.L. Li, Y.B. Chen et al., MOF-derived porous hollow Ni/C composites with optimized impedance matching as lightweight microwave absorption materials. *Adv. Compos. Hybrid Mater.* **4**(3), 707–715 (2021). <https://doi.org/10.1007/s42114-021-00307-z>
7. X.L. Wu, K. Liu, J.W. Ding, B.J. Zheng, F. Gao et al., Construction of Ni-based alloys decorated sucrose-derived carbon hybrid towards: effective microwave absorption application. *Adv. Compos. Hybrid Mater.* **5**(3), 2260–2270 (2022). <https://doi.org/10.1007/s42114-021-00383-1>
8. R.B.J. Chandra, B. Shivamurthy, S.B.B. Gowda, M.S. Kumar, Flexible linear low-density polyethylene laminated aluminum and nickel foil composite tapes for electromagnetic interference shielding. *Eng. Sci.* **21**, 777 (2022)
9. X.L. Cao, Z.R. Jia, D.Q. Hu, G.L. Wu, Synergistic construction of three-dimensional conductive network and double heterointerface polarization via magnetic FeNi for broadband microwave absorption. *Adv. Compos. Hybrid Mater.* **5**(2), 1030–1043 (2022). <https://doi.org/10.1007/s42114-021-00415-w>
10. H.R. Cheng, Z.L. Lu, Q.S. Gao, Y. Zuo, X.H. Liu et al., PVDF-Ni/PE-CNTs composite foams with Co-continuous structure for electromagnetic interference shielding and photo-electro-thermal properties. *Eng. Sci.* **16**, 331–340 (2021)
11. Y.F. Wang, P. Wang, Z.R. Du, C.T. Liu, C.Y. Shen et al., Electromagnetic interference shielding enhancement of poly(lactic acid)-based carbonaceous nanocomposites by poly(ethylene oxide)-assisted segregated structure: a comparative study of carbon nanotubes and graphene nanoplatelets. *Adv. Compos. Hybrid Mater.* **5**(1), 209–219 (2021). <https://doi.org/10.1007/s42114-021-00320-2>
12. T.Q. Hou, Z.R. Jia, A.L. Feng, Z.H. Zhou, X.H. Liu et al., Hierarchical composite of biomass derived magnetic carbon framework and phytic acid doped polyaniline with prominent electromagnetic wave absorption capacity. *J. Mater. Sci. Technol.* **68**, 61–69 (2021). <https://doi.org/10.1016/j.jmst.2020.06.046>
13. J.L. Fan, W.J. Xing, Y. Huang, J.X. Dai, Q. Liu et al., Facile fabrication hierarchical urchin-like C/NiCo₂O₄/ZnO composites as excellent microwave absorbers. *J. Alloys Compd.* **821**, 153491 (2020). <https://doi.org/10.1016/j.jallcom.2019.153491>
14. M. Qin, L.M. Zhang, H.J. Wu, Dual-template hydrothermal synthesis of multi-channel porous NiCo₂O₄ hollow spheres as high-performance electromagnetic wave absorber. *Appl. Surf. Sci.* **515**, 146132 (2020). <https://doi.org/10.1016/j.apsusc.2020.146132>
15. J.W. Wen, X.X. Li, G. Chen, Z.N. Wang, X.J. Zhou et al., Controllable adjustment of cavity of core-shelled Co₃O₄@NiCo₂O₄ composites via facile etching and deposition for electromagnetic wave absorption. *J. Colloid Interface Sci.* **594**, 424–434 (2021). <https://doi.org/10.1016/j.jcis.2021.03.056>
16. J.Q. Wang, J.Q. Ren, Q. Li, Y.F. Liu, Q.Y. Zhang et al., Synthesis and microwave absorbing properties of N-doped carbon microsphere composites with concavo-convex surface. *Carbon* **184**, 195–206 (2021). <https://doi.org/10.1016/j.carbon.2021.08.021>
17. K. Yadav, R. Bagal, S. Parmar, T.U. Patro, A.C. Abhyankar, In situ coating of needle-like NiCo₂O₄ magnetic nanoparticles on lightweight reticulated vitreous carbon foam toward achieving improved electromagnetic wave absorption. *Ind. Eng. Chem. Res.* **60**(39), 14225–14238 (2021). <https://doi.org/10.1021/acs.iecr.1c02636>
18. H.J. Wu, M. Qin, L.M. Zhang, NiCo₂O₄ constructed by different dimensions of building blocks with superior electromagnetic wave absorption performance. *Compos. Part B* **182**, 107620 (2020). <https://doi.org/10.1016/j.compositesb.2019.107620>
19. Y. Guo, D.D. Wang, T.T. Bai, H. Liu, Y.J. Zheng et al., Electrostatic self-assembled NiFe₂O₄/Ti₃C₂T_x MXene nanocomposites for efficient electromagnetic wave absorption at ultralow loading level. *Adv. Compos. Hybrid Mater.* **4**(3), 602–613 (2021). <https://doi.org/10.1007/s42114-021-00279-0>
20. Y. Mu, L. Zhang, H. Liu, H. Wu, Regulating pH value synthesis of NiCo₂O₄ with excellent electromagnetic wave absorbing performance. *J Mater Sci Mater Electron* **32**(21), 26059–26073 (2021). <https://doi.org/10.1007/s10854-021-06055-6>
21. L. Chai, Y.Q. Wang, Z.R. Jia, Z.X. Liu, S.Y. Zhou et al., Tunable defects and interfaces of hierarchical dandelion-like NiCo₂O₄ via Ostwald ripening process for high-efficiency electromagnetic wave absorption. *Chem. Eng. J.* **429**, 132547 (2022). <https://doi.org/10.1016/j.cej.2021.132547>
22. X.J. Zhou, J.W. Wen, Z.N. Wang, X.H. Ma, H.J. Wu, Size-controllable porous flower-like NiCo₂O₄ fabricated via sodium tartrate assisted hydrothermal synthesis for lightweight electromagnetic absorber. *J. Colloid Interface Sci.* **602**, 834–845 (2021). <https://doi.org/10.1016/j.jcis.2021.06.083>
23. M. Qin, L.M. Zhang, X.R. Zhao, H.J. Wu, Defect induced polarization loss in multi-shelled spinel hollow spheres for electromagnetic wave absorption application. *Adv. Sci.* **8**(8), 2004640 (2021). <https://doi.org/10.1002/advs.202004640>
24. X.G. Su, J. Wang, X.X. Zhang, Z.J. Liu, W. Dai et al., Construction of sandwich-like NiCo₂O₄/Graphite nanosheets/NiCo₂O₄ heterostructures for a tun-able microwave absorber. *Ceram. Int.* **46**(11), 19293–19301 (2020). <https://doi.org/10.1016/j.ceramint.2020.04.269>
25. C.X. Hou, W.Y. Yang, X.B. Xie, X.Q. Sun, J. Wang et al., Agaric-like anodes of porous carbon decorated with MoO₂ nanoparticles for stable ultralong cycling lifespan and high-rate lithium/sodium storage. *J Colloid Interface Sci.* **596**, 396–407 (2021). <https://doi.org/10.1016/j.jcis.2021.03.149>
26. K. Li, Y. Shen, L.H. Xu, H. Pan, N. Shen et al., Achieving electromagnetic wave absorption capabilities by fabrication of flower-like structure NiCo₂O₄ derived from low-temperature co-precipitation. *Vacuum* **205**, 111493 (2022). <https://doi.org/10.1016/j.vacuum.2022.111493>
27. C.X. Hou, W.Y. Yang, H. Kimura, X.B. Xie, X.Y. Zhang et al., Boosted lithium storage performance by local build-in electric field derived by oxygen vacancies in 3D holey N-doped carbon



- structure decorated with molybdenum dioxide. *J. Mater. Sci. Technol.* **142**, 185–195 (2023). <https://doi.org/10.1016/j.jmst.2022.10.007>
28. C.X. Hou, Y. Hou, Y.Q. Fan, Y.J. Zhai, Y. Wang et al., Oxygen vacancy derived local build-in electric field in mesoporous hollow Co_3O_4 microspheres promotes high-performance Li-ion batteries. *J. Mater. Chem. A* **6**(16), 6967–6976 (2018). <https://doi.org/10.1039/C8TA00975A>
29. Q. Mu, R.L. Liu, H. Kimura, J.C. Li, H.Y. Jiang et al., Supramolecular self-assembly synthesis of hemoglobin-like amorphous CoP@N , P-doped carbon composites enable ultralong stable cycling under high-current density for lithium-ion battery anodes. *Adv. Compos. Hybrid Mater.* **6**, 23 (2023). <https://doi.org/10.1007/s42114-022-00607-y>
30. C. Li, Y. Ge, X. Jiang, Z. Zhang, L. Yu, The rambutan-like $\text{C@NiCo}_2\text{O}_4$ composites for enhanced microwave absorption performance. *J Mater Sci Mater Electron* **30**, 3124–3136 (2019). <https://doi.org/10.1007/s10854-018-00592-3>
31. X.F. Liu, C.C. Hao, H. Jiang, M. Zeng, R.H. Yu, Hierarchical $\text{NiCo}_2\text{O}_4/\text{Co}_3\text{O}_4/\text{NiO}$ porous composite: a lightweight electromagnetic wave absorber with tunable absorbing performance. *J. Mater. Chem. C* **5**(15), 3770–3778 (2017). <https://doi.org/10.1039/C6TC05167G>
32. F. Li, Q. Li, H. Kimura, X. Xie, X. Zhang, N. Wu, C. Hou, Morphology controllable urchin-shaped bimetallic nickel-cobalt oxide/carbon composites with enhanced electromagnetic wave absorption performance. *J Mater Sci Technol* **148**, 250–259 (2023)
33. Y. Wu, K.H. Tian, R.W. Shu, J.B. Zhu, Y. Liu et al., Constructing interpenetrating structured $\text{NiCo}_2\text{O}_4/\text{HCNT}$ composites with heterogeneous interfaces as low-thickness microwave absorber. *J. Colloid Interface Sci.* **616**, 44–54 (2022). <https://doi.org/10.1016/j.jcis.2022.02.027>
34. N. Zhang, P.Z. Chen, W.X. Chen, Y. Wang, Multi-components matching construction of $\alpha\text{-[SiW}_{11}\text{Mn}(\text{H}_2\text{O})\text{O}_{39}]^{6-}$ /biacid codoped polyaniline wrapped interstice skeletal NiCo_2O_4 for high-performance electromagnetic wave absorption. *Compos. Sci. Technol.* **204**, 108643 (2021). <https://doi.org/10.1016/j.compscitech.2020.108643>
35. C.X. Hou, F.S. Li, H. Kimura, Q.Y. Li, L.Y. Liu et al., Sodium chloride assisted synthesis of porous magnetic carbon nanocomposites containing cobalt nanoparticles for high-performance electromagnetic wave-absorption. *J. Mater. Res. Technol.* **25**, 5148–5158 (2023). <https://doi.org/10.1016/j.jmrt.2023.07.010>
36. M. Qin, H.S. Liang, X.R. Zhao, H.J. Wu, Filter paper templated one-dimensional $\text{NiO/NiCo}_2\text{O}_4$ microrod with wide-band electromagnetic wave absorption capacity. *J. Colloid Interface Sci.* **566**, 347–356 (2020). <https://doi.org/10.1016/j.jcis.2020.01.114>
37. Y.Y. Dong, X.J. Zhu, F. Pan, L. Cai, H.J. Jiang et al., Implanting NiCo_2O_4 equalizer with designable nanostructures in agaric aerogel-derived composites for efficient multiband electromagnetic wave absorption. *Carbon* **190**, 68–79 (2022). <https://doi.org/10.1016/j.carbon.2022.01.008>
38. F.S. Li, Z.Y. Bi, H. Kimura, H.Y. Li, L.Y. Liu et al., Energy- and cost-efficient salt-assisted synthesis of nitrogen-doped porous carbon matrix decorated with nickel nanoparticles for superior electromagnetic wave absorption. *Adv. Compos. Hybrid Mater.* **6**, 133 (2023). <https://doi.org/10.1007/s42114-023-00710-8>
39. S.S. Wang, H.H. Zhu, Q.Z. Jiao, X.G. Jiao, C.H. Feng et al., Controllable synthesis of multi-shelled $\text{SiO}_2@\text{C@NiCo}_2\text{O}_4$ yolk-shell composites for enhancing microwave absorbing properties. *New J. Chem.* **45**(44), 20928–20936 (2021). <https://doi.org/10.1039/D1NJ03897D>
40. W. Wang, H. Zhang, Y.Z. Zhao, J.N. Wang, H.T. Zhao et al., A novel MOF-driven self-decomposition strategy for $\text{CoO@N/C-Co/Ni-NiCo}_2\text{O}_4$ multi-heterostructure composite as high-performance electromagnetic wave absorbing materials. *Chem. Eng. J.* **426**, 131667 (2021). <https://doi.org/10.1016/j.cej.2021.131667>
41. M. Srivastava, K. Surana, P.K. Singh, R. Ch, Nickel oxide embedded with polymer electrolyte as efficient hole transport material for perovskite solar Cell. *Eng Sci* **17**, 216–223 (2021)
42. X.B. Xie, B. Zhang, Q. Wang, X.H. Zhao, D. Wu et al., Efficient micro-wave absorber and supercapacitors derived from puffed-rice-based biomass carbon: effects of activating temperature. *J Coll Interface Sci.* **594**, 290–303 (2021). <https://doi.org/10.1016/j.jcis.2021.03.025>
43. M. Qin, L.M. Zhang, H.J. Wu, Dielectric loss mechanism in electromagnetic wave absorbing materials. *Adv. Sci.* **9**(10), 2105553 (2022). <https://doi.org/10.1002/adv.202105553>
44. M.L. Ma, W.T. Li, Z.Y. Tong, Y. Ma, Y.X. Bi et al., NiCo_2O_4 nanosheets decorated on one-dimensional $\text{ZnFe}_2\text{O}_4@\text{SiO}_2@\text{C}$ nanochains with high-performance microwave absorption. *J. Colloid Interface Sci.* **578**, 58–68 (2020). <https://doi.org/10.1016/j.jcis.2020.05.044>
45. S.J. Zhang, B. Cheng, Z.R. Jia, Z.W. Zhao, X.T. Jin et al., The art of framework construction: hollow-structured materials toward high-efficiency electromagnetic wave absorption. *Adv. Compos. Hybrid Mater.* **5**(3), 1658–1698 (2022). <https://doi.org/10.1007/s42114-022-00514-2>
46. H.L. Xing, J.X. Xie, M.Q. Hu, Sheet-like NiCo_2O_4 -interconnected multiwalled carbon nanotubes with high-performance electromagnetic wave absorption. *J. Mater. Sci. Mater. Electron.* **33**(1), 306–320 (2021). <https://doi.org/10.1007/s10854-021-07294-3>
47. Q. Chang, H.S. Liang, B. Shi, H.J. Wu, Sodium oxalate-induced hydrothermal synthesis of wood-texture-column-like NiCo_2O_4 with broad bandwidth electromagnetic wave absorption performance. *J. Colloid Interface Sci.* **600**, 49–57 (2021). <https://doi.org/10.1016/j.jcis.2021.05.019>